Terahertz microcavity quantum-cascade lasers

Cite as: Appl. Phys. Lett. **87**, 211112 (2005); https://doi.org/10.1063/1.2136222
Submitted: 16 May 2005 • Accepted: 03 October 2005 • Published Online: 17 November 2005

G. Fasching, A. Benz, K. Unterrainer, et al.

Terahertz microcavity quantum-cascade lasers

G. Fasching,[a] A. Benz, and K. Unterrainer
Institute of Photonics and Center for Micro- and Nanostructures, Vienna University of Technology, Floragasse 7, A-1040 Vienna, Austria

R. Zobl, A. M. Andrews, T. Roch, W. Schrenk, and G. Strasser
Institute of Solid State Electronics and Center for Micro- and Nanostructures, Vienna University of Technology, Floragasse 7, A-1040 Vienna, Austria

(Received 16 May 2005; accepted 3 October 2005; published online 17 November 2005)

We demonstrate circular-shaped microcavity quantum-cascade lasers emitting in the THz region between 3.0 and 3.8 THz. The band structure design of the GaAs/$Al_{0.15}Ga_{0.85}As$ heterostructure is based on longitudinal-optical phonon scattering for depopulation of the lower radiative state. A double metal waveguide is used to confine the whispering gallery modes in the gain medium. The threshold current density is 900 A/cm^2 at 5 K. Lasing takes place in pulsed-mode operation up to a heat-sink temperature of 140 K. © *2005 American Institute of Physics*. [DOI: 10.1063/1.2136222]

In recent years, terahertz (THz) quantum-cascade lasers (QCLs) have been successfully realized and subsequently explored.[1–3] THz-QCLs provide a compact source of coherent electromagnetic radiation that can be used in a wide field of applications, including imaging, spectroscopy, and sensing. The successful development and the wide range of possible applications of these edge-emission lasers, draw the attention to realize circular microcavities emitting in the THz frequency region. Microresonators are of interest for fundamental studies of cavity quantum electrodynamics concerning enhanced quantum efficiency and a reduction of the laser threshold.[4] Beside this, large arrays of compact and individually controllable microcavities could be realized on one chip without cleaving or edge polishing. The uncontrollable directionality of the microresonators can be circumvented by the use of smoothly deformed cavities, which yield output power enhancement due to high output directionality.[5,6] In THz-QCLs the vertical confinement is usually achieved by metallic confinement,[7] which yields very high confinement values and low optical loss. These waveguides are not restricted by a cutoff wavelength for the TM polarized intersubband radiation and allow the realization of very thin waveguides. Therefore, it is very interesting to fabricate THz microresonator lasers using double plasmon vertical confinement in contrast with the dielectric confinement used in conventional semiconductor lasers and in mid-infrared QCLs. Due to the metallic confinement electrical biasing and thermal heat sinking are maintained. Together with lateral photonic bandgap structures THz microresonators could lead to strong coupling effects. In this Letter we present the realization of the first double plasmon circular microresonator laser working in the THz regime. The threshold current is as low as 0.9 kA/cm^2 and the highest operating temperature reaches 140 K.

The band structure design of the $Al_{0.15}Ga_{0.85}As$/GaAs laser structure (Fig. 1) is nominally identical to the four-quantum-well THz-QCl scheme introduced by Williams.[3,8] In contrast to Ref. 8 we use on top of the 60 nm thick upper contact layer a thin $In_{0.5}Ga_{0.5}As$ layer to achieve a nonalloyed Ohmic contact and the 155 Å wide GaAs well is doped $n_d=1.25\times10^{16}$ cm^{-3}. Band structure calculations yield two upper $s=4$, 3 and two lower $s=2$, 1 states. This causes two competing lasing transitions with matrix elements $z_{42}>z_{32}$ at $F<10.5$ kV/cm and $z_{32}>z_{42}$ at $F>10.5$ kV/cm, yielding emission of $\nu>3$ THz for low electric fields and $\nu<3.8$ THz for high electric fields. The one-dimensional (1-D) calculation of the waveguide yields a modal confinement $\Gamma=0.98$ and a waveguide loss $\alpha_w=25.9$ cm^{-1} with a 60 nm thick top and a 300 nm thinned bottom contact layer at 3.1 THz. The waveguide losses are mainly caused by the confining top and bottom gold layers. The resulting effective refractive index $n_{\text{eff}}=3.5$ will be considered further on in the analysis of the spectra from the microcavities. The depopulation takes place via fast LO-phonon scattering from the lower laser states $s=1$, 2 into the injector states of the adjacent module.

The heterostructure was grown by molecular-beam epitaxy on a semi-insulating GaAs substrate with 177 cascaded modules. The growth sequence starts with a 100 nm undoped $Al_{0.55}Ga_{0.45}As$ etch stop layer, followed by the 800 nm $n_d=3\times10^{18}$ cm^{-3} doped bottom contact layer. After the subsequent growth of the 177 modules the $n_d=5\times10^{18}$ cm^{-3} doped 60 nm top contact was grown, which was covered by a thin $In_{0.5}Ga_{0.5}As$ layer. We processed the QCL devices into a double metal configuration, which causes a high modal confinement and drastically reduces the free carrier losses.

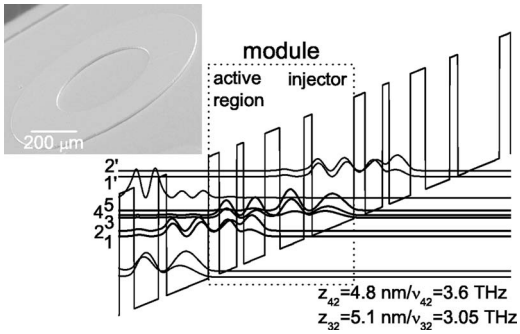

FIG. 1. Conduction band of the four-well structure using a 1-D Schrödinger solver at an electric field $F=10.6$ kV/cm, which corresponds to 57.2 mV/module. Starting at the right-hand injector well, the layer thicknesses in Å are 155/41/65/25/79/55/90/30. The inset shows a scanning electron micrograph of a ring cavity ($R_{\text{out}}=400$ μm/$R_{\text{in}}=200$ μm).

[a]Electronic mail: gernot.fasching@tuwien.ac.at

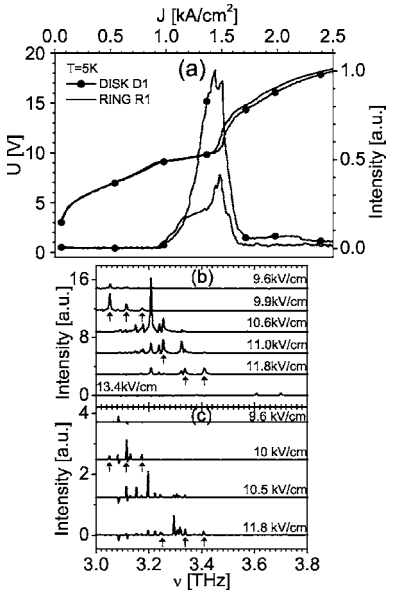

FIG. 2. (a) Emission intensity and applied voltage U versus current density J of the microdisk D1 ($R_{out}=200\ \mu m$) and microring R1 ($R_{out}=200\ \mu m/R_{in}=100\ \mu m$). (b), (c) Background-corrected spectra of microdisk D1 and microring R1 at increasing applied electric field F showing emission between 3.0 and 3.8 THz. The linewidths are limited by the spectrometer resolution (3.75 GHz) and shifted vertically for clarity.

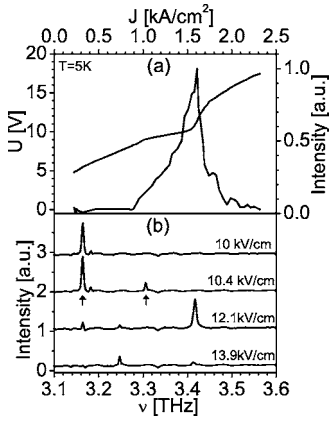

FIG. 3. (a) Emission intensity and applied voltage U versus current density J of the microdisk D2 ($R_{out}=100\ \mu m$) at 5 K. (b) Background-corrected spectra of the microdisk at various applied electric fields F.

Wafer pieces of the MBE-grown material and of an n^+ GaAs substrate were covered with Ti/Au (10 nm/1200 nm). After aligning each GaAs substrate piece upside down on the metallized surface of the laser material, the samples were bonded at 330 °C for 30 min under constant pressure in a commercial wafer bonder. After removing the substrate and the $Al_{0.55}Ga_{0.45}As$ etch stop layer of the MBE-grown material,[7] the 800 nm thick n^+ layer was etched down to 300 nm to reduce free carrier absorption. Afterward, the Ti/Au (10 nm/600 nm) top contact layers were deposited by sputtering. The contact layers as a self-aligned etch mask and an inductively coupled $SiCl_4/N_2$ plasma (ICP) were used to etch down the active region to the wafer-bonded Ti/Au layers. This resulted in perpendicular and smooth resonator boundaries with metal confinement over the whole gain medium. After soldering the chip onto a copper plate and wire bonding, the devices were mounted on the cold finger of a helium-flow cryostat.

The spectra of microdisks labeled D1 and D2 with an outer radius $R_{out}=200\ \mu m$ and $R_{out}=100\ \mu m$ as well as a microring labeled R1 with an outer radius $R_{out}=200\ \mu m$ and an inner radius $R_{in}=100\ \mu m$ were measured. The devices were operated in pulsed mode with 100 ns long pulses at a repetition rate of 1 kHz for the integral measurements and at a repetition rate of 5 kHz for the measurements of the spectra. The emission was measured using a nitrogen-purged Fourier transform infrared (FTIR) spectrometer (NICOLET Magna IR 850) equipped with a Si beamsplitter and a 4.2 K Si bolometer. The spectra were measured in linear scan mode with a resolution of 0.125 cm^{-1} (3.75 GHz). Lasing of the microdisk D1 and the microring R1 starts at 900 A/cm^2 and reaches the maximum at about 1.5 kA/cm^2 [see Fig. 2(a)]. The U-J curve shows two clear kinks, the first one when the structure is aligned and starts lasing ($F=9.4$ kV/cm) and the second one when the structure starts to misalign ($F=10.7$ kV/cm). The clear reduction of the differential resistivity is due to the enhanced current flow as a consequence of the stimulated emission.[9] Microdisk cavities support two distinctly different resonant mode types.[10,11] One mode type is called the radial mode that strikes the disk boundary close to normal incidence and the wave motion is directed along the radial direction. The effective optical path of this mode type is ideally $L_r=2rn_{eff}$,[12] where r and n_{eff} are the radius and the effective refractive index of the cavity. The other resonance mode type is called the whispering gallery mode (WGM).[13] The light is confined by total internal reflection at the outer perimeter of the gain medium, which leads to an effective optical path of $L_w=2r\pi n_{eff}$. The ratio of the optical paths L_w/L_r causes a mode spacing ratio $\Delta\lambda_w/\Delta\lambda_r=\pi$.[12] Generally, when analyzing the spectra of a microdisk resonator, one has to consider that the spectra are a superposition of radial- and WG-type modes. Figures 2(b) and 2(c) shows the corresponding spectra for increasing applied electric field F at 5 K. The spectrum of the microdisk D1 in Fig. 2(b) shows a single mode emission at 3.05 THz for $F=9.6$ kV/cm and changes to multimode emission with increasing field F. At 10.6 kV/cm, where the matrix elements z_{42} and z_{32} of the two lasing transitions are comparable, we observe the maximum intensity. Above 10.7 kV/cm the intensity and the number of modes decrease. At $F=13.4$ kV/cm weak modes at 3.61 and 3.7 THz are observed. The broad emission range is due to the two competing laser transitions and is in good agreement with our band structure calculations. The spectra of the microring R1 in Fig. 2(c) show the same qualitative behavior of the modes with increasing electric field, like the microdisk D1 in Fig. 2(b). The modes of the microring R1 can be attributed to WG-type modes. The modes that can be found in D1 and R1 are marked with an arrow. Assuming periodic boundary conditions, the mode spacing in the frequency spectrum is given by $\Delta\nu_{w,r}=c/L_{w,r}$, where c is the vacuum speed of light and $L_{w,r}$ is calculated using a constant $n_{eff}=3.5$ as a result of our waveguide calculations. If we calculate the mode spacing, we get $\Delta\nu_r=214$ GHz and $\Delta\nu_w=68$ GHz. The mode spacing of the marked modes from left to right in Fig. 2(b) is 62 GHz, 62 GHz, 79 GHz, 81 GHz, 74 GHz and in Fig. 2(c) is 65 GHz, 68 Ghz, 79 GHz, 86 GHz, 70 GHz. The measured mode spacings are roughly comparable to the calculated $\Delta\nu_w$.

We have also measured the intensity and the voltage-current density characteristic as well as the spectra of a microdisk labeled D2 with an outer radius $R_{out}=100\ \mu m$ [Figs.

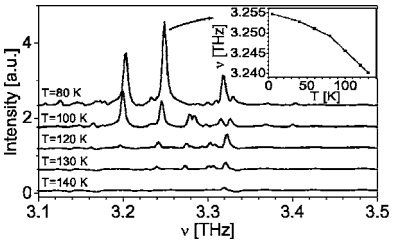

FIG. 4. Temperature dependence of the emission spectra of the microdisk D1. The current density was kept constant at $J=1.62$ kA/cm^2. The inset shows the redshift of the mode around 3.25 THz between 5 and 130 K.

3(a) and 3(b)]. Emission starts, compared to the microdisk D1 in Fig. 2(a), also approximately at 900 A/cm^2 ($F=9.4$ kV/cm) and reaches the maximum at 1.6 kA/cm^2. The *U-J* characteristic of the microresonator D2 shows, like D1, a decrease of the slope due to lasing until the structure starts to misalign at $F=10.9$ kV/cm. The reduction of the mode volume causes a reduction of the possible modes, as can be seen in Fig. 3(b) compared to Fig. 2(b). The mode spacing of the two with an arrow marked modes in Fig. 3(b) is 144 GHz, which is comparable to the calculated mode spacing $\Delta\nu_w=136$ GHz of WG-type modes.

In addition, we have studied the temperature dependence of the microdisk D1. Figure 4 shows the spectra of the microdisk in pulsed-mode operation between 80 and 140 K for a constant current density of $J=1.6$ kA/cm^2. We observe a redshift of the individual modes as well as an overall shift of the emission to higher frequencies with increasing temperature. The redshift of the modes, which is plotted for the mode around 3.24 THz in the inset of Fig. 3, can be attributed to a change of the refractive index. The relative change $(\nu_2-\nu_1)/\nu_1(T_2-T_1)$ of the selected mode between 80 and 130 K is -5.6×10^{-5} K^{-1}, which is comparable to the change of the refractive index of GaAs of 4.5×10^{-5} K^{-1}.[14] The thermal expansion would cause a shift that would be more than one order of magnitude smaller.[14] The overall blueshift of the emission is due to mode hopping caused by a blueshift of the gain. This shift of the gain to higher energies is attributed to a Stark shift of the lasing transition due to a change of the field distribution.

In summary, we reported the realization of circular-shaped microresonators emitting between 3.0 and 3.8 THz. The measured frequency spacing of the modes that are present in both disks and rings is comparable to the WG-type mode spacing with an optical path $L_w=2r\pi n_{\text{eff}}$. Lasing action of a microdisk with $R_{\text{out}}=200$ μm was observed up to 140 K. This shows together with the low threshold current that THz-QCL microdisks with vertical metallic confinement exhibit very good optical confinement while maintaining excellent heat sinking probabilities.

This work was partly supported by the the Austrian Science Fund FWF (SFB-ADLIS), the EC (TERANOVA, POISE), and the Society for Microelectronics (GME, Austria).

[1]R. Köhler, A. Tredicucci, F. Beltram, H. E. Beere, E. H. Linfield, A. G. Davis, D. A. Ritchie, R. C. Jotti, and F. Rossi, Nature (London) **417**, 156 (2002).
[2]G. Scalari, L. Ajili, J. Faist, H. Beere, E. Linfield, D. Ritchie, and G. Davies, Appl. Phys. Lett. **82**, 3165 (2003).
[3]B. S. Williams, H. Callebaut, S. Kumar, Q. Hu, and J. L. Reno, Appl. Phys. Lett. **82**, 1015 (2003).
[4]Y. Yamamoto and R. E. Slusher, Phys. Today **46**, 66 (1993).
[5]C. Gmachl, F. Capasso, E. E. Narimanov, J. U. Nöckel, A. D. Stone, J. Faist, D. L. Sivco, and A. Y. Cho, Science **280**, 1556 (1998).
[6]S. Gianordoli, L. Hvozdara, G. Strasser, W. Schrenk, J. Faist, E. Gornik, IEEE J. Quantum Electron. **36**, 458 (2000).
[7]B. S. Williams, S. Kumar, H. Callebaut, Q. Hu, and J. L. Reno, Appl. Phys. Lett. **83**, 2124 (2003).
[8]S. Kumar, B. S. Williams, S. Kohen, Q. Hu, and J. L. Reno, Appl. Phys. Lett. **84**, 2494 (2004).
[9]C. Sirtori, F. Capasso, J. Faist, A. L. Hutchinson, D. L. Sivco, and A. Y. Cho, IEEE J. Quantum Electron. **34**, 1722 (1998).
[10]N. C. Frateschi and A. F. J. Levi, J. Appl. Phys. **80**, 644 (1996).
[11]A. Shaw, B. Roycroft, J. Hegarty, D. Labilloy, H. Benisty, C. Weisbuch, T. F. Krauss, C. J. M. Smith, R. Stanley, R. Houdré, and U. Oesterle, Appl. Phys. Lett. **75**, 3051 (1999).
[12]R. A. Mair, K. C. Zeng, J. Y. Lin, H. X. Jiang, B. Zhang, L. Dai, A. Botchkarev, W. Kim, H. Morkoç, and M. A. Kahn, Appl. Phys. Lett. **72**, 1530 (1998).
[13]Lord Rayleigh, in *Scientific Papers* (Cambridge University Press, Cambridge, UK, 1912), Vol. 5, pp. 617–620.
[14]J. S. Blakemore, J. Appl. Phys. **53**, 123 (1982).